Mathematical Biosciences and Engineering

MBE, 20(11): 20245–20273.
DOI: 10.3934/mbe.2023896
Received: 25 June 2023
Revised: 05 September 2023
Accepted: 18 September 2023
Published: 07 November 2023

http://www.aimspress.com/journal/MBE

Research article

Effective multi-class lung disease classification using the hybrid feature engineering mechanism

Binju Saju[1], Neethu Tressa[1], Rajesh Kumar Dhanaraj[2,*], Sumegh Tharewal[2], Jincy Chundamannil Mathew[1] and Danilo Pelusi[3]

[1] Department of Master of Computer Applications, New Horizon College of Engineering, Bengaluru, India
[2] Symbiosis Institute of Computer Studies and Research (SICSR), Symbiosis International (Deemed University), Pune, India
[3] Department of Communication Sciences, University of Teramo, Teramo, Italy

* **Correspondence:** Email: sangeraje@gmail.com.

Abstract: The utilization of computational models in the field of medical image classification is an ongoing and unstoppable trend, driven by the pursuit of aiding medical professionals in achieving swift and precise diagnoses. Post COVID-19, many researchers are studying better classification and diagnosis of lung diseases particularly, as it was reported that one of the very few diseases greatly affecting human beings was related to lungs. This research study, as presented in the paper, introduces an advanced computer-assisted model that is specifically tailored for the classification of 13 lung diseases using deep learning techniques, with a focus on analyzing chest radiograph images. The work flows from data collection, image quality enhancement, feature extraction to a comparative classification performance analysis. For data collection, an open-source data set consisting of 112,000 chest X-Ray images was used. Since, the quality of the pictures was significant for the work, enhanced image quality is achieved through preprocessing techniques such as Otsu-based binary conversion, contrast limited adaptive histogram equalization-driven noise reduction, and Canny edge detection. Feature extraction incorporates connected regions, histogram of oriented gradients, gray-level co-occurrence matrix and Haar wavelet transformation, complemented by feature selection via regularized neighbourhood component analysis. The paper proposes an optimized hybrid model, improved Aquila optimization convolutional neural networks (CNN), which is a combination of optimized CNN and DENSENET121 with applied batch equalization, which provides novelty for the model compared with other similar works. The comparative evaluation of classification performance among CNN,

DENSENET121 and the proposed hybrid model is also done to find the results. The findings highlight the proposed hybrid model's supremacy, boasting 97.00% accuracy, 94.00% precision, 96.00% sensitivity, 96.00% specificity and 95.00% F1-score. In the future, potential avenues encompass exploring explainable machine learning for discerning model decisions and optimizing performance through strategic model restructuring.

Keywords: chest X-ray; lung disease; otsu; contrast limited adaptive histogram equalization; Canny edge detection; DENSENET121; batch equalization; Aquila optimizer

1. Introduction

Today, especially in the medical field, digital image processing has been significant in the diagnosis and classification of various diseases. Information technology, along with electronic healthcare systems, has gained significant relevance in the medical industry in recent years since it aids practitioners in giving patients the best care possible [1]. Accurate analysis of images related to the medical field, including cancer and tumor detection, segmentation and quantification, is crucial in case of clinical level of applications [2]. The classification of medical images has been recognized as one of the necessary applications of artificial intelligence in the world of healthcare. Numerous studies are also seeking to automate medical diagnosis or e-warning jobs using deep-learning algorithms, which have good levels of performance like a human [3].

A vital and significant step in the diagnosis and treatment process is medical imaging. The technical person in the medical team will examine the gathered data and then generate a report describing the things that are noticed in the examination. The referring doctor will go through the report and prescribe a treatment plan based on these photos and the technical person's findings that were filed. Medical imaging is typically required with the scientific procedure for confirming the efficacy of the therapy [4]. X-ray analysis is a typical diagnostic that aids in evaluating various disorders. X-ray is a radiation type that is like visible light. X-rays have high energy levels so they can penetrate through many objects easily. X-rays can generate images of various body parts like tissues, organs and bones on matter like film [5]. An images is taken by the X-ray machine by passing electromagnetic rays of high energy through the particular body part for which the image needs to be recorded. Several studies have investigated the relationship between machine learning strategies for the prediction of diagnostic information from X-ray images. This is a critical moment to address this issue given the control of computers and the vast amounts of records that are available to the public without restriction. There are many advances in X-ray that have helped in producing high quality X-ray images [6].

X-ray of the human chest is one among the most efficient medical modes of diagnosis to identify various chest related diseases. After the COVID-19 pandemic, the World Health Organization (WHO) has reported that patients suffering from various lung diseases have exponentially increased. Many researchers started focusing mainly on diagnosis and effective classification of lung diseases only. Because of the above-mentioned features, chest X-ray was the main resource for classification procedures according to the researchers. The identifiable diseases from chest X-rays vary from COVID-19, presence of nodules, cardiomegaly, pneumonia, hernia, fibrosis, edema, emphysema, consolidation, pneumothorax, pleural thickening, effusion, presence of mass to infiltration. Since various diseases can be identified in a chest X-ray, medical experts can confuse the exact identity of the

disease. One solution for this problem is to create a more efficient deep learning-based model to give diagnosis suggestions to the medical expert.

The main motive of the optimization task is to find the best possible partition that will increase the throughput as well as minimize the communication cost between the accelerators while completing the training of deep neural networks (DNN). It also minimizes the training error. There are a lot of hyper parameters in machine learning and deep learning models, and the setting of these hyper parameters will have a huge impact on the model. The traditional trial and error and enumeration methods are inefficient in setting parameters. An effective way to solve this problem is to introduce an intelligent optimization algorithm to optimize the hyper-parameters of the model to improve the prediction accuracy.

Aquila optimizer (AO) has the advantages of strong global detection ability, high search efficiency and fast convergence speed [7].The AO algorithm is a typical swarm intelligence (SI) algorithm optimized by simulating four predator-prey behaviors of Aquila through four strategies: selecting the search space by high soar with a vertical stoop; exploring within a divergent search space by contour flight with a short glide attack; exploiting within a convergent search space via low flight with a slow descent attack; and swooping, walking and grabbing prey. The effect of the Levy flight function makes Aquila search insufficient in the solution space and it tends to fall into local optima. It also leads to a weak local exploitation ability. The traditional AO algorithm uses the rand function to initialize the population position randomly, which cannot ensure uniform distribution of the solution space, and thus reduces the efficiency of the algorithm.

In this work, chest X-Ray images from a reliable open-source dataset will be the input to the model and after performing necessary pre-processing, potential features will be extracted and feature selection will be done. With the help of the efficient classification model thus built, the lung diseases can be effectively classified. The remaining structure of the article is arranged as: Section 2 gives the recent related research works; research gap and contributions are explained in Section 3; Section 4 shows materials and methods used, which include the dataset used and various steps involved in the proposed methodology; Section 5 illustrates experimentation and analysis of the work, which include experimental setup, parameters and performance evaluation, and finally conclusions and future scope is discussed in Section 6.

2. Related works

Deep learning has completely restructured the computer vision field by enabling highly accurate and efficient image recognition, object detection and segmentation. Overall, deep learning has enabled significant advances in computer vision, enabling highly accurate and efficient recognition, detection and segmentation of objects within images. Artificial neural network (ANN) and DNN are commonly used techniques for classification. The two fundamental steps of the picture preprocessing step are noise removal and image enhancement. Depending on the strength or colors, the segmentation step divides the image into the background and the foreground. Finally, feature extraction is done, which requires condensing the information to just include the most crucial aspects, saving time and money. The study [8] proposed a method that combined a standard type of classifier, the softmax, with a classifier based on a transfer learning algorithm for evaluating the classification efficiency. The method used was to classify tissue in images of cancer. The combination of a support vector machine (SVM) classifier with a softmax connection layer using the transfer learning algorithm improved classification accuracy.

Chowdhury et al. [9] presented a deep convolutional neural network (DCNN) model using a

transfer learning algorithm for computer aided identification of pneumonia. The authors built the model and evaluated the performance using chest X-ray pictures. CheXNet, a variant of DENSENET, fared better than the other networks when picture augmentation was not used. Sreeja et.al. [10] put forward a deep learning-based model that will detect the presence of COVID-19 in the chest X-ray of a patient. They used a CNN model along with a histogram of oriented gradients (HOG). The proposed model was compared with various statistical methods and performance was analyzed. The proposed model obtained an accuracy of 92.95%, recall of 85.00% and precision of 91.50%, which is more effective than the compared models and other models in the literature study.

Soni et al. [11] proposed a hybrid model to properly diagnose pulmonary disease, which is considered as one of the most widespread diseases in the world. This disease generally affects lungs as blockage due to other lung diseases. The work combined space transformer network and CNN and named the model as space transformer network convolutional neural network (STNCNN). The model was implemented using the National Institutes of Health (NIH) chest X-ray dataset, which is openly available in Kaggle. The suggested model was compared with vanilla grey, vanilla red, green and blue (RGB) and CNN models. Using the sample dataset, the proposed model obtained an accuracy of 69.00%, whereas vanilla grey got 67.00% accuracy, vanilla RGB got 69.50% and CNN got 63.80% accuracy. The performance and the execution time was found to be less for the proposed model. Indumathi and Siva [12] proposed a hybrid using mask-regional convolutional neural network (M-RCNN) combined with bidirectional long short term memory (LSTM) and crystal algorithm. Initially the dependencies were done using binary LSTM, which is actually a fully connected layer of M-RCNN. Three datasets: COVID-19 radiograph dataset, Tuberculosis (TB) chest X-ray dataset and NIH chest X-ray dataset were used for training as well as testing the performance of the model. The performance was evaluated for bidirectional long short-term memory (BiLSTM), M-RCNN, long short-term memory (LSTM), BiLSTM + M-RCNN and the proposed hybrid model BiLSTM + M-RCNN + crystal algorithm to obtain accuracy values of 90.54, 89.56, 95.95, 93.53 and 99.00%, respectively. The proposed model performed well in the terms of other performance parameters like precision, specificity and ROC curve.

Shamrat et al. [13] proposed a model termed LungNet22 whose structure is similar to VGG16. The study tried to classify 10 different lung diseases from X-ray images of the chest. The study compared eight deep learning models for classifying lung diseases. It was observed that VGG16 had achieved the highest efficiency in classification, which is 92.95%. Later, Adam optimizer was applied with VGG16 and LungNet22 obtained a higher accuracy of 98.89%. Rajagopal et al. [14] proposed an effective classification model for detecting lung diseases from chest radiograph (CXR) images. The proposed model was implemented using deep convolutional spiking neural network for the detection. The work started with preprocessing using anisotropic diffusion filter based unsharp masking. The noise factor was removed using the crispening scheme. Later, an empirical wavelet transform was applied for extracting the features. Finally, the extracted features were given as input for a discontinuity capturing shallow neural network (DCSNN). Also, the weights of the model were optimized using the arithmetic optimization algorithm (AOA). The proposed model obtained accuracy of 96.65%, specificity of 98.52%, F1 score of 91.09%, recall of 97.74% and precision of 93.61%.

A deep learning method based on transfer learning technique was proposed by Kim et al. [15] to categorize lung illnesses on CXR pictures. The approach is a one-step, end-to-end learning approach, which entails directly feeding raw CXR images into a deep learning model (EfficientNet v2-M) in order to extract their significant characteristics for categorizing diseases. On the three classes of normal, pneumonia and pneumothorax in the American NIH data set, we conducted experiments utilizing our

suggested method, and we obtained validation performances of loss = 0.6933, accuracy = 82.15%, sensitivity = 81.40% and specificity = 91.65%. Testing accuracy for the normal, pneumonia, pneumothorax and tuberculosis classes was 63.60%; sensitivity and specificity were 82.20%, 81.40% and 94.48%. For automatic lung disease categorization from chest X-ray pictures, Farhan and Yang [16] proposed a novel hybrid deep learning algorithm (HDLA) framework. The model includes automatic feature extraction, detection and pre-processing of CXR images. Using extremely effective 1-D feature estimates from the input images, the suggested 2-D CNN model ensures robust feature learning. Min-max scaling is applied to improve the extracted 1-D features because they have large scale variability. According to the findings in the experiment, the suggested model has performed well in case of accuracy with an increase of 3.10% compared to the existing literature.

In a paper by Buragadda et al. [17], the UNET which is a U-shaped encoder-decoder network architecture and cyclic generative adversarial networks (GANs) are combined in an effort to increase the dataset size before executing the multi-classification process. The majority of real-world data is unbalanced, which has an impact on the design's overall architecture and performance. Therefore, by executing segmentation utilizing the UNET operation, the improved cyclic GAN's process aids in the creation of a balanced dataset with more enhanced or reconstructed CXR images. The proposed model, which integrated a semantic segmentation component known as "UNET" instead of trained models, achieved the greatest accuracy of 97.19%, which is around 1.50% higher than the basic model. EfficientNetB0, EfficientNetB1 and EfficientNetB2 pretrained models are the multichannel models employed in a study conducted by Ravi et al. [18]. The characteristics of EfficientNet models are combined. The fused characteristics are then sent via many completely connected non-linear layers. The features were then fed into a classifier for lung disease diagnosis using stacked ensemble learning. Random forest and SVM are used in the early stages of the stacked ensemble learning classifier for lung disease detection, while logistic regression is used in the later stage. For pediatric pneumonia lung disease, TB lung disease and COVID-19 lung illness, the suggested technique has demonstrated detection accuracy of 98.00, 99.00 and 98.00%, respectively.

In a similar work done by Ismael and Şengür [19], the authors proposed a new model based on CNN for diagnosing COVID-19 from CXR images. The model used an image dataset of 200 healthy and 180 COVID-19 chest X-rays. The suggested model used three deep CNN approaches, which are deep feature extraction, fine-tuning and end-to-end training of pre-trained CNN models. Five deep CNN models were applied for specifically deep feature extraction. SVM classifier was used with four kernel functions for classification of deep features. The deep features that were extracted by merging SVM classifier to the ResNet50 model along with the linear kernel function generated an accuracy score of 94.70%. The fine-tuning of the ResNet50 model was seen as 92.60%, whereas the 91.60% result was produced by end-to-end training of the new CNN model. In this work, deep learning approaches were seen to be outperformed.

In a study conducted by Blain et al. [20], it was suggested that for determining the severity of lung diseases including COVID-19, application of deep learning approaches and tools on chest X-ray images were viable. The study was carried out on 65 chest X-rays from a hospital in Italy, under the review of two radiologists, out of which 48 images were of COVID-19 patients. In this work, deep learning models were used for lung segmentation as well as detecting opacity level. They used Cohen's kappa analysis for interpretation and got 0.51 kappa concordance for alveolar opacities and also interstitial opacities of 0.71. They could also show that the severity of lung opacities was related to increased age, multimorbidity and necessity of taking precautions.

Further studies were done to find other related works, which were varying from the methods used, the diseases classified and identified and also the accuracy percentage attained. Usage of hybrid quantum-classical CNN gave 98.60% [21], deep CNN model gave 97.80% [22], DFC mechanism along with CNN gave 96.00% [23], GAN along with transfer learning and LSTM gave 99.00% [24], DENSENET121, Mobile Net and NasNet models based on optimistic prediction majority gave 100.00% [25], a combination of five different pre-trained CNN models on three different datasets gave 96.10, 99.50 and 99.70%, respectively [26], and four different pre-trained deep learning models gave 99.31, 98.61, 97.22 and 95.13%, respectively [27].

3. Research motivations

The different diseases that can be identified from chest X-rays are pneumothorax, consolidation, infiltration, emphysema, atelectasis, effusion, fibrosis, pneumonia, pleural thickening, hernia, cardiomegaly, nodule mass and edema. After conducting a thorough literature study on the similar recent works conducted from 2020 onwards, the following research gaps were identified:

1) It was observed that the highest accuracy obtained for classifying maximum among all the before-mentioned thirteen types of lungs diseases is 82.15%, which could be increased for more efficient classification [8–12].

2) The research also identified the presence of over-fitting and under-fitting in the existing models, which could be eliminated [13–15].

3) Accuracy was very low for models that were classifying lung diseases to very few classes which were not acceptable accuracy percentage [16–19].

4) The datasets studied with existing models had less observations, which can directly or indirectly affect the quality of work [20–23].

5) The majority of the similar deep learning models were not satisfactory in enhancing the image quality of X-rays [24–26].

6) Most of the existing works were following feature engineering mechanisms that could be made hybrid with the help of employing multiple feature engineering mechanisms for improving accuracy.

3.1. Contributions

Machine learning-based models can be a powerful tool for predicting diagnostic information from X-rays. It can be an efficient mode for predicting diagnostic information from X-ray images, but it requires careful data collection, preprocessing, feature extraction and model selection, as well as rigorous testing and validation to ensure that the model is accurate and reliable. In view with the research gaps identified, the proposed work provides the following contributions:

1) Since the images in the dataset are of different size, a proper image resizing is done to make the images uniform before further processing, which can eventually result in justifiable observations.

2) Otsu algorithm is used for binary conversion of images, as it makes the machine learning models more effective than non-converted images.

3) X-ray images have a lot of speckle noise, which will affect the efficiency of classification. Noise removal is done using contrast limited adaptive histogram equalization (CLAHE), which is one of the effective algorithms for speckle noise removal.

4) During the process of classification of images, the most significant feature is detection of edges. Canny edge detector is used for the extraction of the edges of the images.
5) Feature extraction is one of the important steps in the proposed methodology. Potential set of features such as shape, texture and wavelength were extracted with the following robust techniques: shape feature using connected regions and HOG, texture feature using gray-level co-occurrence matrix (GLCM), wavelet feature using Haar wavelet transformation (HWT).
6) Regularized neighborhood component analysis (RNCA) is applied for feature selection.
7) Optimized hybrid model consisting of CNN, DENSENET121, along with batch equalization was used for a novel classification of thirteen types of lung diseases from the X-ray image of lungs.

4. Material and methods

4.1. Dataset

For medical imaging diagnosis, chest X-ray scanning is the most commonly used and cheapest method available till now. But because of the non-uniformity in chest X-ray scan images, it becomes difficult for direct processing of the images. The National Institutes of Health (NIH) Clinical Center released an open-source dataset for clinical researchers for aiding computing machines with artificial intelligence for effectively diagnosing and classifying various diseases. This dataset was made available publicly via https://nihcc.app.box.com/v/ChestXray-NIHCC/folder/36938765345. The NIH chest X-ray dataset consists of twelve files that have around 112,120 images, which are taken from the X-ray of 30,805 patients. The images cover 14 classes, which include 13 different lung diseases like pneumothorax, consolidation, infiltration, emphysema, atelectasis, effusion, fibrosis, pneumonia, pleural thickening, hernia, cardiomegaly, nodule mass and edema and normal lungs images.

The effectiveness of the classification increases with the number of images in the dataset and also the amount of pre-processing and quality enhancement of images. Before the NIH clinical center released this dataset, the only large available open-source dataset was provided by Openi with only 4143 images. The resource unavailability for labeling large number of images was the crucial cause behind the lack of large datasets. In the NIH dataset, the labeling was done using natural language processing (NLP) and text-mine disease classifications from related laboratory documents. The labels are found to be more than 90.00% accurate and best fit for supervised learning. The sample labeled dataset is provided in Figure 1.

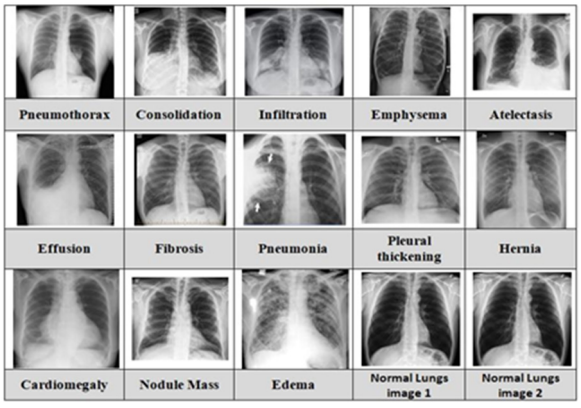

Figure 1. Sample labeled images from data set.

The dataset was divided into two splits. 77.00% of the data (86,524 images) were utilized for training and the remaining 23.00% of data (25,596 images) for testing. The data table based on the observations from radiographical reports along with corresponding frequency is drawn as in Table 1.

Table 1. Observations from the dataset.

Sl No	Labels	Observations	Frequency
1	No Finding	60,361	0.426468
2	Infiltration	19,894	0.140557
3	Effusion	13,317	0.0940885
4	Atelectasis	11,559	0.0816677
5	Nodule/Mass	12,113	0.0447304
6	Pneumothorax	5302	0.0374602
7	Consolidation	4667	0.0329737
8	Pleural_Thickening	3385	0.023916
9	Cardiomegaly	2776	0.0196132
10	Emphysema	2516	0.0177763
11	Edema	2303	0.0162714
12	Fibrosis	1686	0.0119121
13	Pneumonia	1431	0.0101104
14	Hernia	227	0.00160382

4.2. Methods

General machine learning pipeline was adopted for the study, which is described in detail in the later sections. The machine learning pipeline begins with reading of data, followed by various preprocessing techniques including gray scale conversion, image resizing, image conversions, removal of noise, enhancement of image and detection of edges and patterns [28,29]. After employing the necessary pre-processing techniques using various algorithms, the features were extracted and selected, which are sent to the model. The model is then well-trained with the data and then tested. The performance is evaluated after the testing of the models using the performance analysis matrices including accuracy, sensitivity, precision, specificity and F1-score. Figure 2 explains the general pipeline of machine learning architecture used in the proposed work.

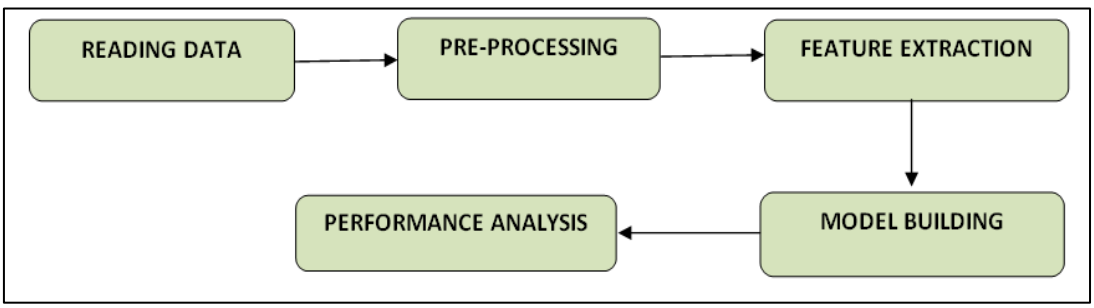

Figure 2. Proposed method.

4.3. Proposed classification framework

Machine learning has been vital to classify lung disorders and to improve the precision and effectiveness of identifying lung diseases such pneumonia, TB, lung cancer, etc. Figure 3 portrays the methodology that has been followed in the work, which reads the chest X-ray images, followed by pre-processing, feature extraction, feature selection, classification and performance evaluation.

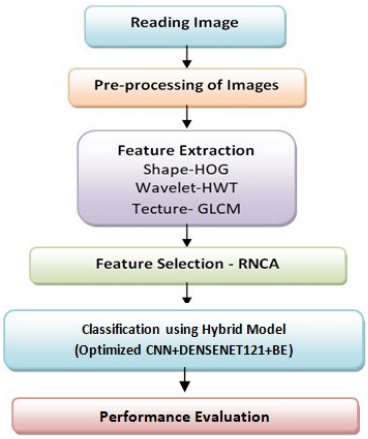

(a)

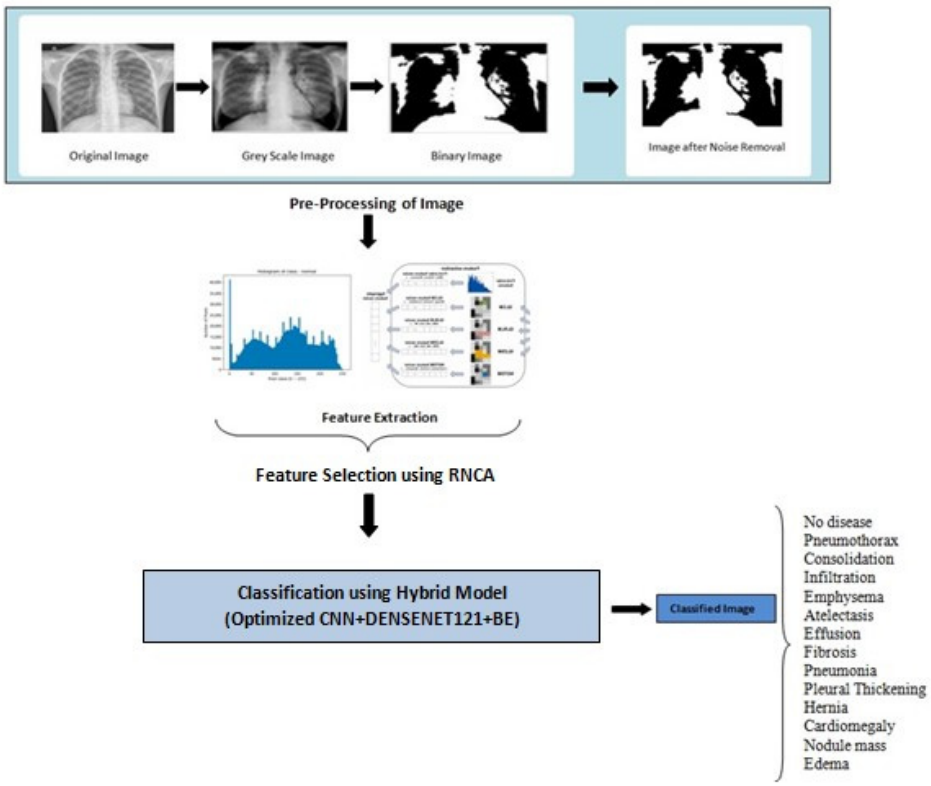

(b)

Figure 3. (a) Proposed methodology; (b) Proposed classification framework.

4.4. Image pre-processing

Pre-processing is considered as the most significant part in every classification model, as it enhances the quality of input, thereby improving the output quality. Figures 4 and 5 depict the pre-processing steps followed in this work.

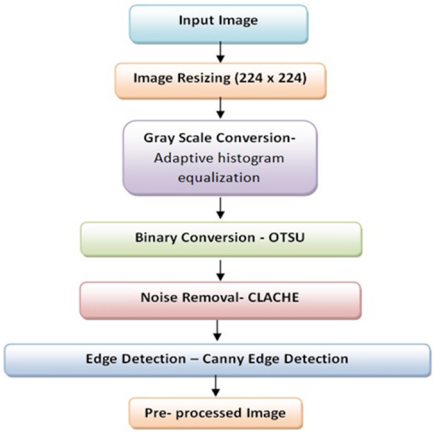

Figure 4. Pre-processing of the data.

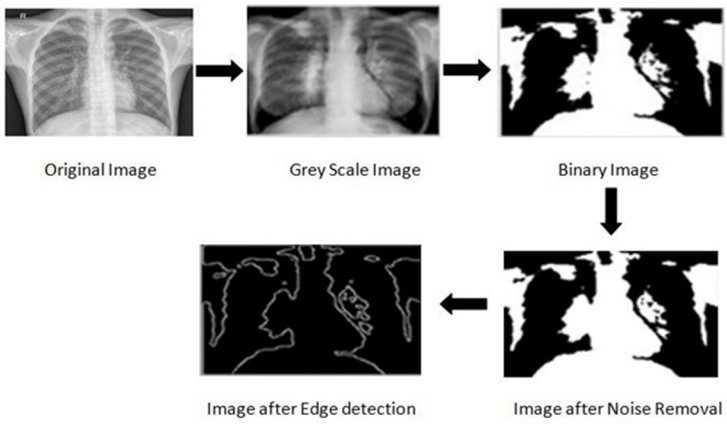

Figure 5. Pre-processing of the data objects.

4.4.1. Image resizing

Image resizing is a common pre-processing step in machine learning that involves altering the size of an image while preserving its aspect ratio. Image resizing aids in improving the training speed as well as in bringing uniformity to the input data. Resizing of images has enhanced the accuracy of the model in many studies. In this work, all the images of chest X-rays are resized into 224 × 224 pixels for constructing the model much faster and easier as follows:

$$J = imresize(I, [224, 224]). \quad (1)$$

This method accepts the image pixels count corresponding to the number of rows and columns

and converts the image to a resized image with 224 rows and columns.

4.4.2. Grayscale conversion

Grayscale conversion is a common pre-processing step in image analysis and computer vision applications. It abridges the algorithm and requires less computation. It involves altering a color image to a grayscale image, where each pixel in the grayscale image indicates the brightness of the corresponding pixel in the color image. The steps involved in grayscale conversion are given as follows:
1) Scan the image to extract RGB color components from input image into 3 2D matrices;
2) Create a zero matrix with same order of that of the RGB image;
3) Convert each pixel value to grayscale value using weighted sum method on corresponding pixel position such as (i,j) as follows:

$$grayscale\ value\ at\ (i,j) = 0.299\ \times\ R(i,j) + 0.587 \times G(i,j) + 0.114 \times B(i,j). \quad (2)$$

Adaptive histogram equalization is employed in this study to convert the input images into grayscale-based images as in Figure 6. This will improve the contrast through several histograms by redistributing the image luminance values.

Figure 6. Pre-processing of the data objects.

4.4.3. Binary conversion

Otsu's method is a widely used technique for thresholding grayscale images to change them into binary images [30]. The binary image consists of pixels that are either white (with a value of 1) or black (with a value of 0), based on whether their intensity values exceed a certain threshold value. Otsu's method involves finding the best threshold value which separates the grayscale image. The particular threshold value is chosen such that the variance between the two classes is maximized, while the variance within each class is minimized. Here are the steps involved in Otsu's method for thresholding a grayscale image:
1) Histogram representation of the grayscale image showing the distribution of pixel intensities is formed
2) Normalize the histogram to determine the probability distribution function (PDF).
3) Calculate cumulative distribution function (CDF) of the PDF.
4) Find the mean intensity value of the image collection.
5) For each possible threshold value, calculate the between-class variance.

6) Choose the threshold value that maximizes the between-class variance.

$$\sigma^2(t) = w_0(t)\sigma_0^2(t) + w_1(t)\sigma_1^2(t), \tag{3}$$

where w_0 and w_1 are the probabilities of 2 classes with threshold t, which are calculated from the L-bins of the histogram as shown below:

$$w_0(t) = \sum_{i=0}^{t-1} p(i), \tag{4}$$

$$w_1(t) = \sum_{i=t}^{L-1} p(i). \tag{5}$$

Once the optimal threshold value has been determined, the grayscale form of the image can be converted into the binary format of the image by setting the intensity value of each pixel to 1 if its intensity value exceeds the threshold, and otherwise 0.

4.4.4 Noise removal

CLAHE is an efficient algorithm for noise removal [31]. To reduce noise presence in the images, we used the CLAHE method along with high boost filtering. The proposed technique employs an effective filter chain, which consist of a sound absorption filter, a high pass filter and a CLAHE filter, to process the 2D X-ray images. For X-ray images in 2D format, the approach automatically and without user intervention enhances the contrast. In order to facilitate accurate diagnosis, tissue contrast will be given that is customized for each treatment.

The CLAHE algorithm enhances the image quality based on clip limit as well as tile size, following Rayleigh distribution as given below:

$$pixelvalue(j) = pixelvalue \sqrt{2\ (\lambda^2)\ ln\left(1 - \frac{1}{1-sum(j)}\right)}_{min}, \tag{6}$$

where $pixelvalue_{min}$ is a lower limit of pixel value, λ is Rayleigh's parameter for scaling and $sum(j)$ is the cumulative probability.

4.4.5. Edge detection

Canny edge detection is one of the best edge detecting algorithms for detecting edges in X-ray images [32]. The first step of the Canny operator edge detection technique is smoothing the image using a Gaussian filter, and the next step is the maximum suppression of the amplitude with the gradient's direction. The third step employs the double threshold technique to identify and detect the edges. Figure 7 depicts the block diagram for these phases.

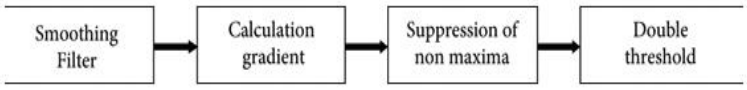

Figure 7. Block diagram of Canny edge detection.

The local gradient amplitude maximum is sought after using the Canny operator edge detection technique. Since the original Canny edge detection algorithm cannot handle color images, it is only utilized

for grayscale images, making it very difficult to determine parameters adaptively. Figure 5 provided in one of the previous sections illustrates the pre-processing followed in the study with sample images.

4.5. Feature extraction

The technology has difficulty in diagnosing chest illness and performs low when the images are sent directly for classification. In order to achieve the best detection results, it is crucial to extract the appropriate features. Based on the literature survey, we identified that shape, texture and wavelet features can be the key features from which lung diseases can be differentiated much better than existing frameworks, which are explained below in detail.

4.5.1. Shape feature extraction

The object retrieval procedure makes use of connected regions, which is ideally suited for obtaining shape information from the input samples [33]. The formulas used to calculate shape features are given in Table 2 and sample histograms are shown in Figure 8.

Table 2. Formulae for shape features extraction from HOG.

Sl No	Feature	Equation
1	Perimeter	$\sum_{i,j=0}^{M,N} E_d\ (i,j)$
2	Area	$\sum_{i,j=0}^{M,N} b\ (i,j)$
3	Circularity	$\frac{4\pi A}{P^2}$

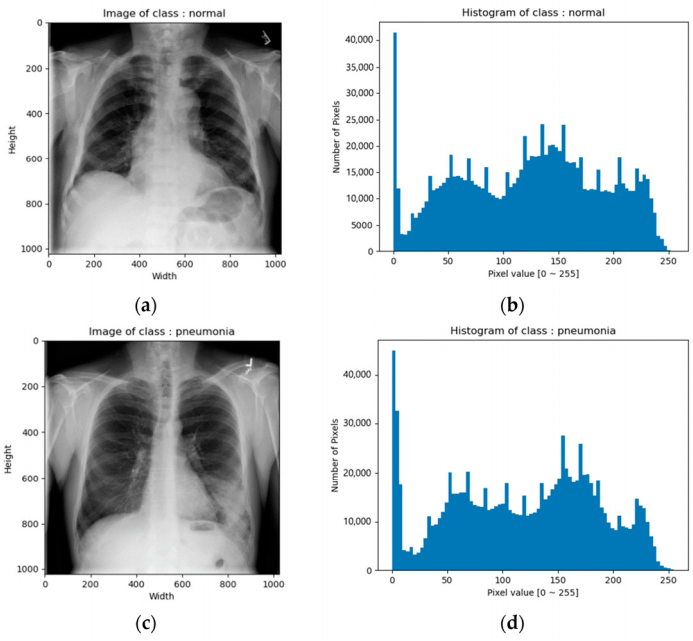

Figure 8. (a) Normal lungs; (b) histogram of normal; (c) pneumonia; (d) histogram of pneumonia.

4.5.2. Texture feature extraction

Gray level co-occurrence matrix (GLCM) is an effective method for text feature extraction from X-ray images [34]. The spatial pixel value arrangement of the image corresponds to the texture features. The GLCM approach is preferred by the suggested model to obtain text-based characteristics. The full set of features was composed of textural, first-order, statistical and higher-order textural features based on the GLCM, gray-level run length matrix (GLRLM), gray level size zone matrix (GLSZM) and neighboring gray tone difference matrix (NGTDM) of the image.

The GLCM method determines the precise relationship between two pixels in an image that are separated by a particular amount. The suggested work extracts statistical features from the many features that the GLCM approaches contain. Many features are extracted using the suggested feature extraction techniques, potentially increasing computing complexity. Consequently, choosing an ideal feature collection is crucial for reducing computing complexity. The formulas for feature extraction for this study is shown in Table 3 and the flow is shown in Figure 9.

Table3. Formulas for texture features extraction from GLCM.

Sl No	Feature	Formula
1	Contrast	$\sum_{i,j=0}^{N-1} P_{i,j}\ (i-j)^2$
2	Correlation	$\sum_{i,j=0}^{N-1} P_{i,j}\left[\frac{(i-\mu_i)(j-\mu_j}{\sqrt{(\sigma_i^2)(\sigma_j^2)}}\right]$
3	Energy	$\sum_{i,j=0}^{N-1} P_{i,j}^2$
4	Entropy	$\sum_{i,j=0}^{N-1} P_{i,j}(-\ln P_{i,j})$
5	Mean	$\sum_{i,j=0}^{N-1} i\ (P_{i,j}),\ \mu_j = \sum_{i,j=0}^{N-1} j\ (P_{i,j})$
6	Variance	$\sigma_i^2 = \sum_{i,j=0}^{N-1} P_{i,j}(i-\mu_i)^2,\ \sigma_j^2 = \sum_{i,j=0}^{N-1} P_{i,j}(j-\mu_j)^2$
7	Standard Deviation	$\sigma_j = \sqrt{\sigma_i^2},\ \sigma_j = \sqrt{\sigma_j^2}$

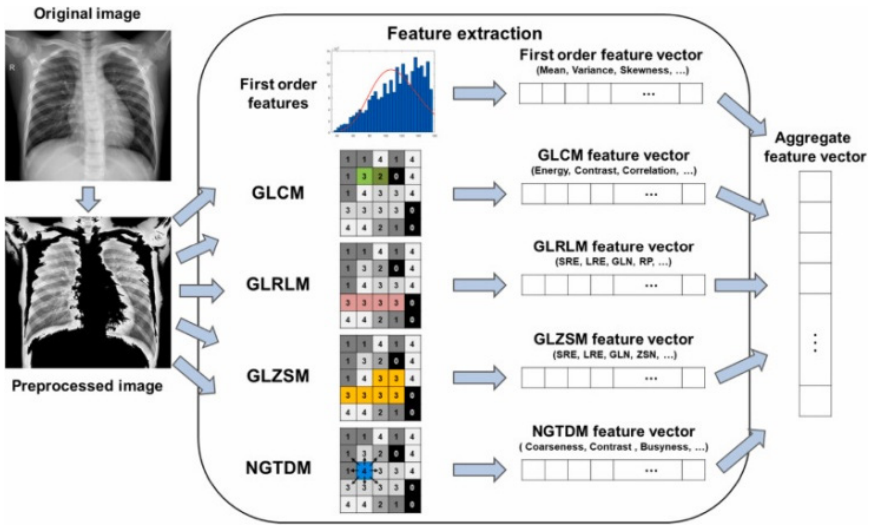

Figure 9. Texture feature extraction.

4.5.3. Wavelet feature extraction

The simplest wavelet transform technique is the Haar transform [35]. Using many stretches and shifts, the HWT technique cross-multiplies a function over the Haar wavelet. The HWT works by dividing an image into smaller sub-regions or blocks, called wavelets. Each wavelet is a scaled and shifted version of a simple waveform, called the mother wavelet. The transformation is carried out in a hierarchical manner, with each level of the transformation generating a set of coefficients that represent the frequency content of the image at that level. The mother wavelet function of Haar wavelet can be described as:

$$\psi(t) = \begin{cases} 1 & 0 \le t < \frac{1}{2}, \\ -1 & \frac{1}{2} \le t < 1, \\ 0 & otherwise \end{cases} \cdot \tag{7}$$

4.6. Feature selection

By selecting the most useful characteristics, selection of features brings down the high data dimensionality [36]. Neighborhood components analysis (NCA) is used for feature selection in the proposed cataract detection method. Using feature weights, this technique can forecast features in the best possible way. This stage's goal is to reduce computing complexity and improve classification accuracy. The multi-level feature selection method called NCA algorithm followed by relief algorithm is the suggested RNCA. The pseudo code of relief and NCA algorithm is shown below (Algorithm 1):

Algorithm 1: Algorithm for RNCA

Input: Extracted features
Output: Reduced features
Featured dimentionality reduction: features, SD, threshold
START
Featureout = feature
for $I = 1$ to m **do** Decision1 = threshold/ featureout[i]: Decision2 = average/featureout[i]
Endfor
If ($Decision1 > threshold$ and $Decision2 > threshold$
Then
featureout[i] = []
Endif
END

By selecting instances at random from the dataset that is given as input to the algorithm, followed by updating each feature and identifying instances that are close to one another based on the differences between the selected instance and two nearby instances of the same and opposite classes based on the threshold value, the selection of relevant features from the input is taken based on the threshold. This method will thus reduce the number of features.

4.7. Model building

There are several machine learning models that can be used to detect images using their features or properties. Our proposed model is a hybrid model that is an optimized CNN_DENSENET121 (densely-connected convolutional neural network) with batch equalization.

The proposed hybrid model is a combination of CNN and DENSENET121. Initially, the CNN gathers the input of selected features and the further processes are performed by DENSENET in the network system. The loss in the network is optimized using the improved Aquila optimization (IAO) technique. The goal of this IAO method is to minimize the loss function through weight parameter update. A convolutional neural network and dense network (CNN + DENSENET121) combination is an effective approach for many modern image recognition tasks. CNN acts as the frontend and DENSENET acts as the backend. The CNN extracts the features by applying relevant filters and the DENSENET analyzes these features, taking into consideration the information received from previous time-steps.

The network starts with the traditional 2D CNN followed by batch normalization, ELU activation, max-pooling and dropout with a dropout rate of 50%. Three such convolutional layers are placed in a sequential manner with their corresponding activations. The convolutional layers are followed by the permute and the reshape layer, which is very necessary as the shape of the feature vector differs from CNN to DENSENET. The convolutional layers are developed on 3D feature vectors, whereas the dense networks are developed on 2D feature vectors. The permute layers change the direction of the axes of the feature vectors, which is followed by the reshape layers, which convert the feature vector to a 2D feature vector. Finally, the output of the bidirectional layers is fed to the time distributed dense layers followed by the fully connected layer.

CNN, a common deep neural network type for image classification, object recognition and other computer vision applications, is the CNN [37]. The input to a CNN model is typically a grayscale or RGB image, which is pre-processed by resizing and normalizing the pixel values to a common scale. The model parameters are updated using backpropagation and are repeated for multiple epochs until the model converges to a stable set of parameters.

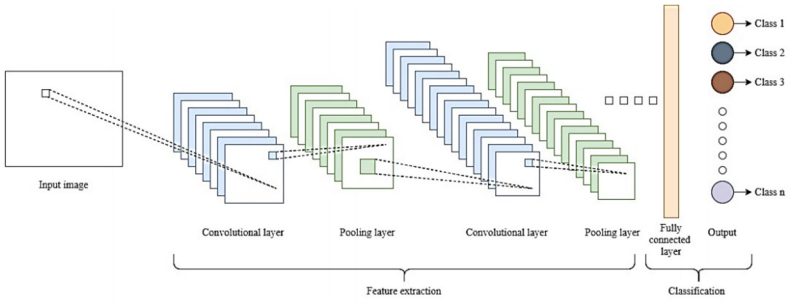

Figure 10. DENSENET121 architecture.

The deep learning network class includes DENSENET. Figure10 narrates the architecture of DENSENET121. There are variations of the DENSENET, including DENSENET-121, DENSENET-160 and DENSENET-201 [38]. The numbers in the name refer to how many layers there are in the neural network. The following are the 121 layers of DENSENET121: basic convolution

layer with 64 filters of size 7 × 7 and a stride of 2, basic pooling layer with 3 × 3 max pooling and a stride of 2, Dense Block 1 with 2 convolutions repeated 6 times, transition layer 1 (1 Conv + 1 AvgPool), Dense Block 2 with 2 convolutions repeated 12 times, transition layer 2 (1 Conv + 1 AvgPool), Dense Block 3 with 2 convolutions repeated 24 times, transition layer 3 (1 Conv + 1 AvgPool), Dense Block 4 with 2 convolutions repeated 16 times, global average pooling layer—accepts all the feature maps of the network to perform classification and output layer.

The DENSENET consists of many Dense-Blocks [39], of which each block has the same dimensions with a different number of filters. It is a crucial step in CNN that the transition layer applies batch normalization via down sampling.

The classification performance of CNN+DENSENET121 is influenced by the available loss function. Thus, the loss function is minimized by updating the weight parameters using the IAO approach [40]. The available loss function is described as

$$L_F = \frac{1}{T}\sum_{i=1}^{T}(a_i - k_i')^2, \tag{8}$$

where T represents the total number of iterations, actual value is signified as a_i and k_i' is the predicted value. The disease in the image are detected based on the objective function [41], which is expressed as

$$Objectivefunction = Min[L_F]. \tag{9}$$

The goal of this IAO method is to minimize the loss function through weight parameter [42] update. This is one of the population-based approaches and is motivated from the hunting behavior of Aquila. Using IAO, the feature initialization is done by

$$features = \begin{bmatrix} l_{1,1} & \cdots & l_{1,j} & l_{1,\text{K-1}} & l_{1,K} \\ l_{2,1} & \cdots & .l_{2,j} & \cdots & l_{2,K} \\ \cdots & \cdots & .l_{i,j} & \cdots & \cdots \\ \vdots & \vdots & \vdots & \vdots & \vdots \\ l_{P-1,1} & \cdots & .l_{P-1,j} & \cdots & l_{P-1,K} \\ l_{P,1} & \cdots & l_{P,j} & l_{P,K-1`} & l_{P,K} \end{bmatrix}. \tag{10}$$

The present feature solution is represented in Eq (10), in which l_j mentions the position of needed features in solution j, P mentions the overall features and the problem size is signified as K. After the operation of initialization, the IAO approach randomly creates the features [43]. It is mentioned as

$$F_{ij} = rand \times (ub_j - lb_j) + LB_j,\ i = 1,2,\ldots,Pj = 1,2,\ldots,K, \tag{11}$$

where ub_j signifies the upper bound in j^{th} position, the lower bound in j^{th} position is indicated as lb_j and $rand$isthe random number. The IAO approach performs four stages like expanded exploration, Narrowed exploration, Weight Strategy and Normalization to obtain the objective function, which are explained in the following subsections.

1) Process of expanded exploration: Here [44], the search agent moves to search the effective features and chooses the optimal set of features for robust cataract detection. It is given as

$$L(h+1) = L_{best}(h) \times \left(1 - \frac{p}{H}\right) + (L_N(h) - L_{best}(h) \times rand), \tag{12}$$

where the next iteration in solution $h$is mentioned as $L(h+1)$, the optimal solution that identify the

important affords the is indicated as $L_{best}(H)$, the high process of exploration is maintained by applying $(1-\frac{p}{H})$, $rand$ is the random distribution ranging from 0 to 1, the present number of iteration is specified as h and the maximum iteration is indicated as H.

$$L_N(h) = \frac{1}{P}\sum_{i=1}^{P} L_i\,(h), \forall j = 1,2,\ldots,P, \tag{13}$$

where P refers to the total features, K mentions the problem size and the present iteration is represented a sh.

2) Narrowed exploration process: In this process [45], the locations of features are efficiently targeted by the search agent. Then, it encircles the important features and selects for the cataract detection process. The formulation for updating the position of the search agent is determined as

$$L_2(h+1) = L_{best}(h) \times \gamma(P) + L_r(h) + (x-y) \times rand, \tag{14}$$

where $L_2(h+1)$ represents the upcoming iteration of solution$h$, P mentions the position of feature, Levy flight distribution function is denoted as $\gamma(P)$, and $L_r(h)$ represents the random solution. Levy flight distribution is computed as

$$\gamma(P) = v \times \frac{g \times \beta}{|\rho|^{\frac{1}{\delta}}}, \tag{15}$$

where $u$specifies the constant value 0.7 and$g$and$\beta$are the random numbers ranging between 0 and 1. The constant term β is computed as

$$\beta = \left[\frac{\eta(1+\delta)\times\sin\left(\frac{\pi\delta}{2}\right)}{\eta\left(\frac{1+\delta}{2}\right)\times\delta\times 2^{\eta-1/2}}\right]. \tag{16}$$

Expanded exploitation: The exploitation process [46] is expanded by the search agent through vertically descending to develop the feature attributes. Then, the search agent begins to choose the features that are appropriate for analyzing the cataract from the given input images. Depending on the size and quality, the search agent can select the features. Furthermore, the features that maintain the fitness function are chosen as optimal.

Narrowed exploitation: Based on the feature's robustness, the search agent can choose the significant features for the process of detection. In the final location, the search agent can select the features.

The computation of quality function [47] is evaluated as

$$Qualityfunction(h) = h^{\frac{2\times rand-1}{(1-H)^2}}, \tag{17}$$

$$R_1 = 2 \times rand - 1, \tag{18}$$

$$R_2 = 2 \times \left(1 - \frac{h}{H}\right), \tag{19}$$

where $Qualityfunction(h)$ mentions the range of the quality function in iteration $h$and the random number ranges from 0 to 1 are denoted as $rand$. The performance of the optimization approach is enhanced by introducing a weight strategy.

3) Weight strategy: Each of the features are in varied position and initially the search space is very large. According to the maximum iteration, the feature's distribution scope is compressed and it generates the search space as small. The proposed optimization algorithm moves in to local optimum due to the reduced feature set. To enhance the different characteristics of features and recover the optimization algorithm from the local optima, the weight factor is applied. In this [48], the objective function is evaluated for each iteration and the attained result from every iteration is compared with each other. By analyzing the best objective function, the optimal solution is obtained. The pseudocode of IAO approach [49] is illustrated in Algorithm 2.

Algorithm 2: AO approach

Initialization of features
Initialize the parameters such as $\boldsymbol{\delta, \gamma, \ldots}$
if (condition is not satisfied) **do**
Compute the objective function using Eq (13)
$\boldsymbol{L_{best}(h)}$ = Determine the robust solution based on the objective function
For $\boldsymbol{(i = 1, 2, \ldots., P)}$ do
Update the current solution $\boldsymbol{L_N(h)}$
Update $\boldsymbol{h, r, R_1, R_2}$ and $\boldsymbol{\gamma(P)}$
If $\boldsymbol{rand \leq 0.5}$ then
Solution update using Eq (14)
If $\boldsymbol{Objfunc(K_1(v+1)) < Objfunc(K(v))}$ **then**
$\boldsymbol{L(h) = L_1(h+1)}$
end if
else
Solution update using Eq (15)
If $\boldsymbol{Objfunc\ (L_2(h+1)) < ObjfuncL(h))}$ **then**
$\boldsymbol{L(h) = L_2(h+1)}$
end if
else
if $\boldsymbol{rand \leq 0.7}$ **then**
Solution update using Eq (16)
if $\boldsymbol{Objfunc(L_3(h+1)) < Objfunc(L(h))}$ **then**
$\boldsymbol{L(h) = L_3(h+1)}$
end if
end if
else
Solution update using Eq (17)
if $\boldsymbol{Objfunc(L_4(h+1)) < Objfunc(L(h))}$ **then**
Using Eq (15), compute quality function
Apply weight strategy using Eq (16)
end if
return

4) Normalization [50] is a procedure to change the value of the numeric variable in the dataset to

a typical scale, without misshaping contrasts in the range of values. The main benefit of batch processing in Machine Learning is that it can improve the accuracy and stability of your model training and optimization. Input at each layer is brightened, which will help in having fixed distributions of inputs that would evacuate the ill impacts of the internal covariate shift.

Normalizing the activations [51] of the earlier layer implies that presumptions the ensuing layer makes about the spread and distribution of inputs during the weight update won't change significantly in any event. This has the impact of stabilizing and accelerating the preparation training procedure of DNN. This normalization of inputs might be applied to the input variable for the first hidden layer or to the activation from a hidden layer for a more profound layer [52]. It tends to be utilized with most deep network types, for example, CNN and DENSENET.

The disease classes ranging from 1 to 14 are not shared uniformly. In the proposed experimental data, the number of images varies in each class. When a mini-batch is designed randomly, the grading model obtains the information from unbalanced occurrences and then it becomes biased. This issue is solved by applying a strategy of batch balancing. The similar number of occurrences are randomly chosen during the construction of a mini-batch, i.e., 25 images from all the groups and generate the batch fully balanced.

Training and validation: The pre-processed and feature-extracted data is then used to train the chosen model. In this study, the dataset is divided into training and testing data. The data is divided in such a way that 80.00% of data (89,696 images) were used for trainings and the remaining 20.00% (22,424 images) for testing its performance.

Model evaluation: Once the model completes the training, its efficiency is checked by providing a test dataset and performance is measured using various evaluation metrics. This is crucial for ensuring that the model can generalize successfully with novel, previously unexplored data. Performance evaluation is discussed in detail in the next section. Overall, machine learning can be a powerful tool for detecting lung diseases, but it requires careful data collection, pre-processing, feature extraction and model selection, as well as rigorous testing and validation to ensure that the model is accurate and reliable.

5. Experimentation, results and analysis

5.1. Experimental setup

The experimental setup is as shown in Figure 11 with 16 GB RAM and Intel Core i5 8th Gen CPU with 3.0 GHz speed. Anaconda 3.0 was used for implementing the proposed scheme.

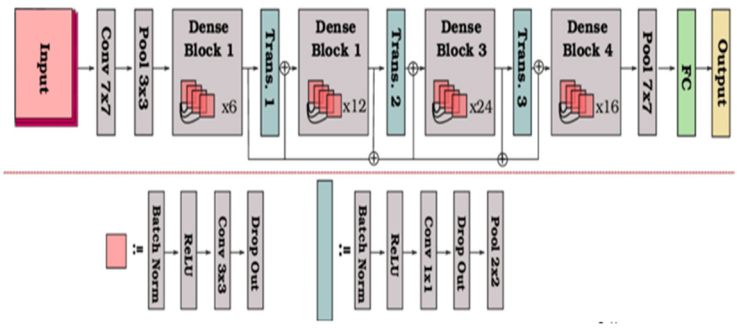

Figure 11. DENSENET121 architecture.

5.2. Experimental parameter

The experimental setup is provided in Table 4. Parameter settings of CNN and DENSENET121 are shown in Table 5.

Table 4. Experimental setup.

Manufacturer	Acer@
Processor	Intel® Core™i5-4670S CPU @3.10GHz
RAM	16.0 GB (15.9 GB usable)
System Type	64-bit Operating System

Table 5. Model parameters.

CNN		DENSENET121	
Number of epochs	20	Number of epochs	10
Iterations	500	Iterations	500
Iteration per epoch	25	Iteration per epoch	50

The efficiency or caliber of the proposed model is assessed using a number of metrics, also known as performance metrics or evaluation metrics. Performance analysis of machine learning models is a crucial step in evaluating the effectiveness and efficiency of the model. It involves measuring the accuracy and other relevant metrics of the performance of the model on a test dataset, which is separate from the dataset used for training the model. In this study, the model performance is evaluated through accuracy, precision, sensitivity and ROC curve for CNN and DENSENET121.

5.3. Performance evaluation

Classification accuracy [53] is the count of predictions done correctly divided by the entire number of predictions, multiplied by 100.

$$Accuracy = \frac{Number\ of\ predictions\ made\ correct}{Total\ number\ of\ predictions}. \tag{20}$$

The precision [54] comes from the proportion based on positive predictions that was actually correct.

$$Precision = \frac{TP}{(TP+FP)}, \tag{21}$$

where TP stands for true positive and FP stands for false positive.

Sensitivity [55] is measured as the proportion based on actual positives identified incorrectly.

$$Sensitivity = \frac{TP}{(TP+FN)}, \tag{22}$$

where FN stands for false negatives.

F1-score [56] is the harmonic mean based on precision and sensitivity.

$$F_1 - score = 2 \times \frac{Pr\,ecision \times Sensitivity}{Pr\,ecision + Sensitivity}. \tag{23}$$

Specificity [57] maps for the number of correct negative predictions divided by the total number of negatives.

$$Specificity = \frac{TN}{(TN+FP)}, \tag{24}$$

where TN stands for true negative.

Performance analysis in terms of accuracy, precision, sensitivity, F1-scoreand specificity of each class is displayed in Figures 12–16 respectively.

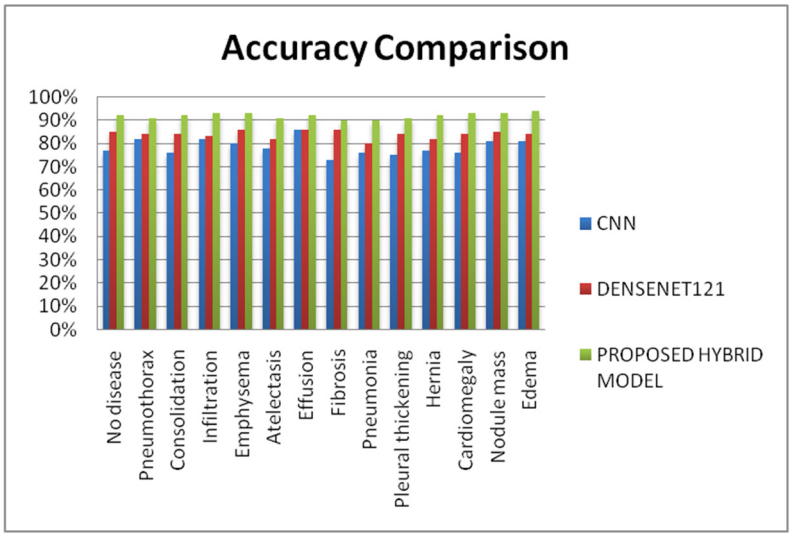

Figure 12. Accuracy comparison of CNN, DENSENET121 and the proposed hybrid model.

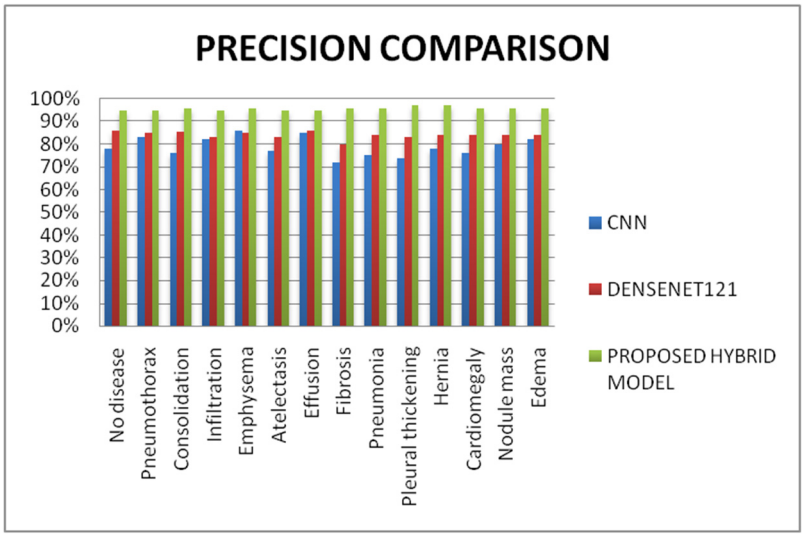

Figure 13. Precision comparison of CNN, DENSENET121 and the proposed hybrid model.

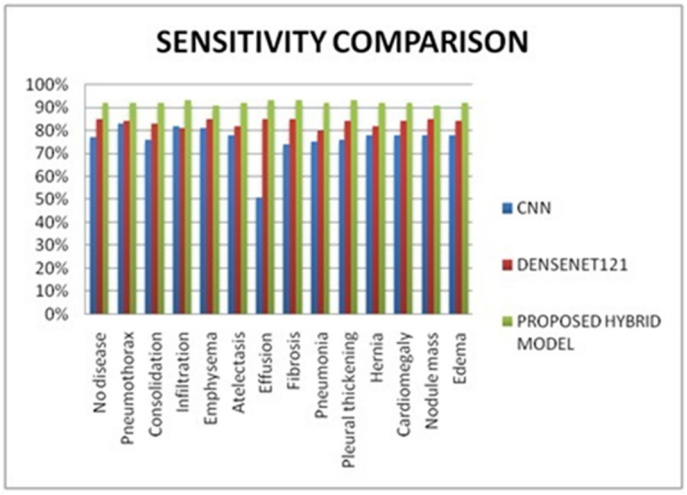

Figure 14. Sensitivity comparison of CNN, DENSENET121 and the proposed hybrid model.

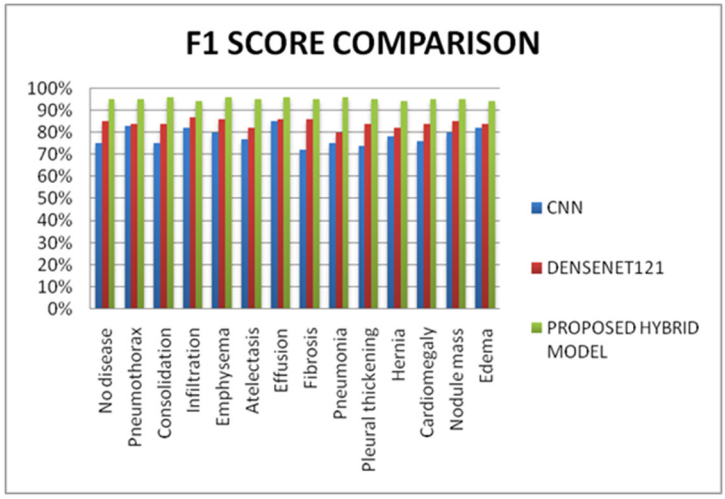

Figure 15. F1-score comparison of CNN, DENSENET121 and the proposed hybrid model.

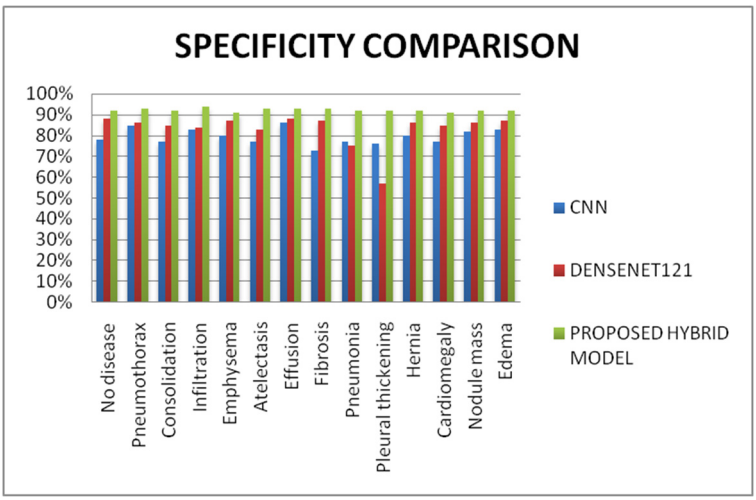

Figure 16. Specificity comparison of CNN, DENSENET121 and the proposed hybrid model.

In the performance analysis, the proposed model is more effective in more than 12 classes of lung disease classification. Overall performance is also analyzed for all three models. Figure 17 shows the overall performance of the three models. The values of various performance metrics obtained by each model are compared.

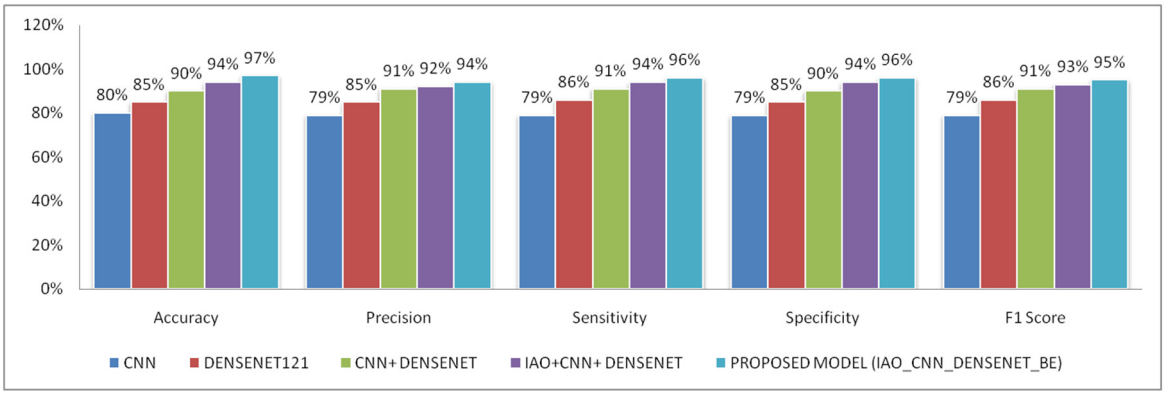

Figure 17. Overall performance comparison.

6. Conclusions and future scope

Medical classification of images is essential to many fields of medical study [58]. This study used deep learning models to create a comprehensive computer-aided model for classifying chest X-ray images. The proposed model is a hybrid model optimized with intelligent AO with batch equivalence applied. Various preprocessing steps were executed to improve the model performance, which include binary conversion using Otsu algorithm, noise removal using CLAHE and edge detection using Canny edge detection. Later, feature extraction was also done, which included extraction of shape features using connected regions, texture features using GLCM, wavelet features using HWT and feature selection done using RNCA. Two well-known deep learning models like CNN and DENSENET121 were implemented for the classification, where DENSENET50 was found to be more effective to classify all the 14 classes with respect to accuracy, precision and sensitivity. DENSENET121 performed with 85.00% of accuracy followed by CNN with 80.00%. Also, DENSENET121 has proven to be more efficient in the terms of precision and sensitivity. It is clearly visible from the study that DENSENET121 is very much effective in classifying the various 13 categories of diseases. Advanced methods like explainable and interpretable machine learning can be used in the future to find the reason for classification based on various features being selected and performance can be further enhanced by restructuring of the model according to the interpretations identified. The proposed model can very well be generalized with any chest X-ray image dataset. Upon the non-availability of the different dataset with all types, we could not test our model for different datasets. The model may not detect existence of more than one lung disease from the input but it will be classified based on highest intensity of infection among the diseases present.

Use of AI tools declaration

The authors declare they have not used Artificial Intelligence (AI) tools in the creation of this article.

Conflict of interest

Danilo Pelusi is an editorial board member for Mathematical Biosciences and Engineering and was not involved in the editorial review or the decision to publish this article. All authors declare that there are no competing interests.

References

1. A. Sinha, A. R P, M. Suresh, N. M. R, A. D, A. G. Singerji, Brain tumour detection using deep learning, in *2021 Seventh International conference on Bio Signals, Images, and Instrumentation (ICBSII)*, (2021), 1–5. https://doi.org/10.1109/ICBSII51839.2021.9445185
2. B. Saju, V. Asha, A. Prasad, V. A, A. S, S. P. Sreeja, Prediction analysis of hypothyroidism by association, in *2023 Third International Conference on Advances in Electrical, Computing, Communication and Sustainable Technologies (ICAECT)*, (2023), 1–6. https://doi.org/10.1109/ICAECT57570.2023.10117641
3. H. Tang, Z. Hu, Research on medical image classification based on machine learning, *IEEE Access*, **8** (2020), 93145–93154. https://doi.org/10.1109/ACCESS.2020.2993887
4. S. K. Zhou, H. Greenspan, C. Davatzikos, J. S. Duncan, B. V. Ginneken, A. Madabhushi, et al., A review of deep learning in medical imaging: Imaging traits, technology trends, case studies with progress highlights, and future promises, *Proc. IEEE*, **109** (2021), 820–838. https://doi.org/10.1109/JPROC.2021.3054390
5. P. Uppamma, S. Bhattacharya, Deep learning and medical image processing techniques for diabetic retinopathy: A survey of applications, challenges, and future trends, *J. Healthcare Eng.*, **2023** (2023), 2728719. https://doi.org/10.1155/2023/2728719
6. Z. Shi, L. He, Application of neural networks in medical image processing, in *Proceedings of the Second International Symposium on Networking and Network Security*, (2010), 23–26.
7. L. Abualigah, D. Yousri, M. A. Elaziz, A. A. Ewees, M. A. A. Al-qaness, A. H. Gandomi, Aquila optimizer: A novel meta-heuristic optimization algorithm, *Comput. Ind. Eng.*, **157** (2021), 107250. https://doi.org/10.1016/j.cie.2021.107250
8. H. Chen, M. M. Rogalski, J. N. Anker, Advances in functional X-ray imaging techniques and contrast agents, *Phys. Chem. Chem. Phys.*, **14** (2012), 13469–13486. https://doi.org/10.1039/c2cp41858d
9. M. E. H. Chowdhury, T. Rahman, A. Khandakar, R. Mazhar, M. A. Kadir, Z. B. Mahbub, et al., Can AI help in screening viral and COVID-19 pneumonia?, *IEEE Access*, **8** (2020), 132665–132676. https://doi.org/10.1109/ACCESS.2020.3010287
10. S. P. Sreeja, V. Asha, B. Saju, P. K. C, P. Manasa, V. C. R, Classifying chest X-rays for COVID-19 using deep learning, in *2023 International Conference on Intelligent and Innovative Technologies in Computing, Electrical and Electronics (IITCEE)*, (2023), 1084–1089. https://doi.org/10.1109/IITCEE57236.2023.10090915

11. M. Soni, S. Gomathi, P. Kumar, P. P. Churi, M. A. Mohammed, A. O. Salman, Hybridizing convolutional neural network for classification of lung diseases, *Int. J. Swarm Intell. Res.*, **13** (2022), 1–15. https://doi.org/10.4018/IJSIR.287544
12. V. Indumathi, R. Siva, An efficient lung disease classification from X-ray images using hybrid Mask-RCNN and BiDLSTM, *Biomed. Signal Process. Control*, **81** (2023), 104340. https://doi.org/10.1016/j.bspc.2022.104340
13. F. M. J. M. Shamrat, S. Azam, A. Karim, R. Islam, Z. Tasnim, P. Ghosh, et al., LungNet22: A fine-tuned model for multiclass classification and prediction of lung disease using X-ray images, *J. Pers. Med.*, **12** (2022), 680. https://doi.org/10.3390/jpm12050680
14. R. Rajagopal, R. Karthick, P. Meenalochini, T. Kalaichelvi, Deep Convolutional Spiking Neural Network optimized with Arithmetic optimization algorithm for lung disease detection using chest X-ray images, *Biomed. Signal Process. Control*, **79** (2023), 104197. https://doi.org/10.1016/j.bspc.2022.104197
15. S. Kim, B. Rim, S. Choi, A. Lee, S. Min, M. Hong, Deep learning in multi-class lung diseases' classification on chest X-ray images, *Diagnostics*, **12** (2022), 915. https://doi.org/10.3390/diagnostics12040915
16. A. M. Q. Farhan, S. Yang, Automatic lung disease classification from the chest X-ray images using hybrid deep learning algorithm, *Multimed. Tools Appl.*, (2023), 38561–38587. https://doi.org/10.1007/s11042-023-15047-z
17. S. Buragadda, K. S. Rani, S. V. Vasantha, M. K. Chakravarthi, HCUGAN: Hybrid cyclic UNET GAN for generating augmented synthetic images of chest X-Ray images for multi classification of lung diseases, *Int. J. Eng. Trends Technol.*, **70** (2020), 249–253. http://doi.org/10.14445/22315381/IJETT-V70I2P227
18. V. Ravi, V. Acharya, M. Alazab, A multichannel Efficient Net deep learning-based stacking ensemble approach for lung disease detection using chest X-ray images, *Cluster Comput.*, **26** (2023), 1181–1203. https://doi.org/10.1007/s10586-022-03664-6
19. A. M. Ismael, A. Şengür, Deep learning approaches for COVID-19 detection based on chest X-ray images, *Expert Syst. Appl.*, **164** (2021), 114054. https://doi.org/10.1016/j.eswa.2020.114054
20. M. Blain, M. T. Kassin, N. Varble, X. Wang, Z. Xu, D. Xu, et al., Determination of disease severity in COVID-19 patients using deep learning in chest X-ray images, *Diagn. Interv. Radiol.*, **27** (2021), 20–27. https://doi.org/10.5152/dir.2020.20205
21. E. H. Houssein, Z. Abohashima, M. Elhoseny, W. M. Mohamed, Hybrid quantum-classical convolutional neural network model for COVID-19 prediction using chest X-ray images, *J. Comput. Design Eng.*, **9** (2022), 343–363. https://doi.org/10.1093/jcde/qwac003
22. W. A. Shalaby, W. Saad, M. Shokair, F. E. A. El-Samie, M. I. Dessouky, COVID-19 classification based on deep convolutional neural networks over a wireless network, *Wireless Pers. Commun.*, **120** (2021), 1543–1563. https://doi.org/10.1007/s11277-021-08523-y
23. W. Saad, W. A. Shalaby, M. Shokair, F. A. El-Samie, M. Dessouky, E. Abdellatef, COVID-19 classification using deep feature concatenation technique, *J. Ambient Intell. Human. Comput.*, **13** (2022), 2025–2043. https://doi.org/10.1007/s12652-021-02967-7
24. S. Sheykhivand, Z. Mousavi, S. Mojtahedi, T. Y. Rezaii, A. Farzamnia, S. Meshgini, et al., Developing an efficient deep neural network for automatic detection of COVID-19 using chest X-ray images, *Alexandria Eng. J.*, **60** (2021), 2885–2903. https://doi.org/10.1016/j.aej.2021.01.011

25. V. Agarwal, M. C. Lohani, A. S. Bist, D. Julianingsih, Application of voting based approach on deep learning algorithm for lung disease classification, in *2022 International Conference on Science and Technology (ICOSTECH)*, (2022), 1–7. https://doi.org/10.1109/ICOSTECH54296.2022.9828806
26. A. Narin, C. Kaya, Z. Pamuk, Automatic detection of coronavirus disease (COVID-19) using X-ray images and deep convolutional neural networks, *Pattern Anal. Appl.*, **24** (2021), 1207–1220. https://doi.org/10.1007/s10044-021-00984-y
27. V. Kumar, A. Zarrad, R. Gupta, O. Cheikhrouhou, COV-DLS: Prediction of COVID-19 from X-rays using enhanced deep transfer learning techniques, *J. Healthcare Eng.*, **2022** (2022), 6216273. https://doi.org/10.1155/2022/6216273
28. Q. Lv, S. Zhang, Y. Wang, Deep learning model of image classification using machine learning, *Adv. Multimedia*, **2022** (2022), 3351256. https://doi.org/10.1155/2022/3351256
29. M. Xin, Y. Wang, Research on image classification model based on deep convolutional neural network, *J. Image Video Process.*, **2019** (2019). https://doi.org/10.1186/s13640-019-0417-8
30. A. H. Setianingrum, A. S. Rini, N. Hakiem, Image segmentation using the Otsu method in Dental X-rays, in *2017 Second International Conference on Informatics and Computing (ICIC)*, (2017), 1–6. https://doi.org/10.1109/IAC.2017.8280611
31. S. Sahu, A. K. Singh, S. P. Ghrera, M. Elhoseny, An approach for de-noising and contrast enhancement of retinal fundus image using CLAHE, *Opt. Laser Technol.*, **110** (2019), 87–98. https://doi.org/10.1016/j.optlastec.2018.06.061
32. S. K. Jadwaa, X-Ray lung image classification using a Canny edge detector, *J. Electr. Comput. Eng.*, **2022** (2022), 3081584. https://doi.org/10.1155/2022/3081584
33. P. G. Bhende, A. N. Cheeran, A novel feature extraction scheme for medical X-ray images, *Int. J. Eng. Res. Appl.*, **6** (2016), 53–60.
34. P. K. Mall, P. K. Singh, D. Yadav, GLCM based feature extraction and medical X-ray image classification using machine learning techniques, in *2019 IEEE Conference on Information and Communication Technology*, (2019), 1–6. https://doi.org/10.1109/CICT48419.2019.9066263
35. S. Gunasekaran, S. Rajan, L. Moses, S. Vikram, M. Subalakshmi, B. Shudhersini, Wavelet based CNN for diagnosis of COVID 19 using chest X ray, in *First International Conference on Circuits, Signals, Systems and Securities*, **1084** (2021). https://doi.org/10.1088/1757-899X/1084/1/012015
36. W. Yang, K. Wang, W. Zuo, Neighborhood component feature selection for high-dimensional data, *J. Comput.*, **7** (2012), 161–168.
37. M. Ramprasath, M. V. Anand, S. Hariharan, Image classification using convolutional neural networks, *Int. J. Pure Appl. Math.*, **119** (2018), 1307–1319.
38. G. Wang, Z. Guo, X. Wan, X. Zheng, Study on image classification algorithm based on improved DENSENET, *J. Phys.: Conf. Ser.*, **1952** (2021), 022011. http://doi.org/10.1088/1742-6596/1952/2/022011
39. N. Hasan, Y. Bao, A. Shawon, Y. Huang, DENSENET convolutional neural networks application for predicting COVID-19 using CT image, *SN Comput. Sci.*, **2** (2021), 389. https://doi.org/10.1007/s42979-021-00782-7
40. B. Sasmal, A. G. Hussien, A. Das, K. G. Dhal, A comprehensive survey on aquila optimizer, *Arch. Comput. Methods Eng.*, **30** (2023), 4449–4476. https://doi.org/10.1007/s11831-023-09945-6
41. S. Ekinci, D. Izci, E. Eker, L. Abualigah, An effective control design approach based on novel enhanced aquila optimizer for automatic voltage regulator, *Artif. Intell. Rev.*, **56** (2023), 1731–1762. https://doi.org/10.1007/s10462-022-10216-2

42. M. H. Nadimi-Shahraki, S. Taghian, S. Mirjalili, L. Abualigah, Binary aquila optimizer for selecting effective features from medical data: A COVID-19 case study, *Mathematics*, **10** (2022), 1929. https://doi.org/10.3390/math10111929
43. A. A. Ewees, Z. Y. Algamal, L. Abualigah, M. A. A. Al-qaness, D. Yousri, R. M. Ghoniem, et al., A cox proportional-hazards model based on an improved aquila optimizer with whale optimization algorithm operators, *Mathematics*, **10** (2022), 1273. https://doi.org/10.3390/math10081273
44. F. Gul, I. Mir, S. Mir, Aquila Optimizer with parallel computation application for efficient environment exploration, *J. Ambient Intell. Human. Comput.*, **14** (2023), 4175–4190. https://doi.org/10.1007/s12652-023-04515-x
45. S. Akyol, A new hybrid method based on Aquila optimizer and tangent search algorithm for global optimization, *J. Ambient Intell. Human. Comput.*, **14** (2023), 8045–8065. https://doi.org/10.1007/s12652-022-04347-1
46. K. G. Dhal, R. Rai, A. Das, S. Ray, D. Ghosal, R. Kanjilal, Chaotic fitness-dependent quasi-reflected Aquila optimizer for superpixel based white blood cell segmentation, *Neural Comput. Appl.*, **35** (2013), 15315–15332. https://doi.org/10.1007/s00521-023-08486-0
47. A. Ait-Saadi, Y. Meraihi, A. Soukane, A. Ramdane-Cherif, A. B. Gabis, A novel hybrid chaotic Aquila optimization algorithm with simulated annealing for unmanned aerial vehicles path planning, *Comput. Electr. Eng.*, **104** (2022), 108461. https://doi.org/10.1016/j.compeleceng.2022.108461
48. S. Wang, H. Jia, L. Abualigah, Q. Liu, R. Zheng, An improved hybrid aquila optimizer and harris hawks algorithm for solving industrial engineering optimization problems, *Processes*, **9** (2021), 1551. https://doi.org/10.3390/pr9091551
49. Y. Zhang, Y. Yan, J. Zhao, Z. Gao, AOAAO: The hybrid algorithm of arithmetic optimization algorithm with aquila optimizer, *IEEE Access*, **10** (2022), 10907–10933. https://doi.org/10.1109/ACCESS.2022.3144431
50. J. Zhong, H. Chen, W. Chao, Making batch normalization great in federated deep learning, preprint, arXiv:2303.06530.
51. M. Segu, A. Tonioni, F. Tombari, Batch normalization embeddings for deep domain generalization, *Pattern Recognit.*, **135** (2023), 109115. https://doi.org/10.1016/j.patcog.2022.109115
52. N. Talat, A. Alsadoon, P. W. C. Prasad, A. Dawoud, T. A. Rashid, S. Haddad, A novel enhanced normalization technique for a mandible bones segmentation using deep learning: batch normalization with the dropout, *Multimed. Tools Appl.*, **82** (2023), 6147–6166. https://doi.org/10.1007/s11042-022-13399-6
53. G. M. M. Alshmrani, Q. Ni, R. Jiang, H. Pervaiz, N. M. Elshennawy, A deep learning architecture for multi-class lung diseases classification using chest X-ray (CXR) images, *Alexandria Eng. J.*, **64** (2023), 923–935. https://doi.org/10.1016/j.aej.2022.10.053
54. F. J. M. Shamrat, S. Azam, A. Karim, K. Ahmed, F. M. Bui, F. De Boer, High-precision multiclass classification of lung disease through customized MobileNetV2 from chest X-ray images, *Comput. Biol. Med.*, **155** (2023), 106646. https://doi.org/10.1016/j.compbiomed.2023.106646
55. K. Subramaniam, N. Palanisamy, R. A. Sinnaswamy, S. Muthusamy, O. P. Mishra, A. K. Loganathan, et al., A comprehensive review of analyzing the chest X-ray images to detect COVID-19 infections using deep learning techniques, *Soft Comput.*, **27** (2023), 14219–14240. https://doi.org/10.1007/s00500-023-08561-7

56. S. Sharma, K. Guleria, A deep learning based model for the detection of pneumonia from chest X-Ray images using VGG-16 and neural networks, *Procedia Comput. Sci.*, **218** (2023), 357–366. https://doi.org/10.1016/j.procs.2023.01.018
57. V. T. Q. Huy, C. Lin, An improved DENSENET deep neural network model for tuberculosis detection using chest X-Ray images, *IEEE Access*, **11** (2023), 42839–42849. https://doi.org/10.1109/ACCESS.2023.3270774
58. V. Sreejith, T. George, Detection of COVID-19 from chest X-rays using ResNet-50, *J. Phys.: Conf. Ser.*, **1937** (2021), 012002. https://doi.org/10.1088/1742-6596/1937/1/012002

AIMS Press

©2023 the Author(s), licensee AIMS Press. This is an open access article distributed under the terms of the Creative Commons Attribution License (http://creativecommons.org/licenses/by/4.0)